J. Fluid Mech. (1976), *vol.* 74, *part* 2, *pp.* 269–295
Printed in Great Britain

The maintenance of turbulent shear stress in a mixing layer

By IAN S. F. JONES
Boeing Scientific Research Laboratories†

(Received 31 May 1974 and in revised form 31 October 1975)

Wavenumber frequency spectra have been measured in a two-dimensional incompressible mixing layer, using linearized hot-wire anemometers. Spectra of two dimensions (frequency and wavenumber) have been measured for lateral and longitudinal turbulent velocities, and used to construct three-dimensional spectra. The validity of the separation assumption used to construct these spectra was tested. Spectra of the velocity product responsible for the mean shear stress and the lateral gradient of this spectrum have been determined, as has a structure constant for the lateral velocity fluctuations that Phillips (1967) suggested is relevant to the maintenance of the shear stress gradient. Phillips' (1967) stress model fails the tests proposed in this study.

1. Introduction

The turbulent shear flows evolve as a result of the erosion of the mean velocity gradient by the turbulent shear stresses, and these stresses also interact with the mean velocity to provide the turbulent energy necessary to sustain the evolution. The earliest models linking the shear stress and the mean velocity gradient by mixing length or eddy diffusivity concepts have proved too simple to be generally applicable. Alternative models relating the shear stress to the other terms in the turbulent energy balance equation require a number of parameters that appear to vary widely from situation to situation. More recently, Phillips (1967) advanced the attractive proposition that the shear stress gradient is related to the second derivative of the mean velocity and structure constants of the lateral velocity fluctuations. It is this model that is examined in this paper.

The shear stress model advanced by Phillips is developed from the work of Miles (1957), who examined water wave generation resulting from wave-induced wind stress. For an inviscid laminar flow, the induced velocity fluctuations due to flow over surface waves bring about an increase in shear stress in the atmosphere at a critical layer where the convection velocity of the disturbance matches the mean velocity. When the air flow is turbulent rather than laminar, a wave-induced stress can be generated outside the critical layer as a result of the induced fluctuations interacting with the atmospheric turbulence.

For turbulent shear flows in general, Phillips (1967) considered perturbations that are Fourier components of the turbulent field, rather than induced by

† Present address: R. A. N. Research Laboratory, Garden Island, N.S.W. 2000, Australia.

surface waves. By arguing that the direct interaction of the lateral velocity fluctuations with the mean flow at the matched layer dominates the maintenance of shear gradient, Phillips' model leads to the convenient expression for shear stress gradient

$$\frac{\partial}{\partial y_2}\overline{u_1 u_2} \propto \beta \overline{u_2^2}\Theta_{22}\frac{\partial^2 U_1}{\partial y_2^2},$$

in terms of β, a structure function, and Θ_{22}, a time scale of the lateral velocity fluctuations u_2.

The above gradient of shear stress is brought about by only those Fourier components of the lateral velocity fluctuations that travel at the local mean velocity. These components induce correlated vorticity fluctuations, so that they can be shown to lead to an increment in shear stress. For lateral velocity fluctuations travelling at other than the local mean, the induced vorticity fluctuations, Phillips argues, are nearly in quadrature with the lateral fluctuations, so there is negligible increment to the shear stress as a result of such components. In a non-turbulent two-dimensional flow, the vorticity and lateral fluctuations would be exactly in quadrature away from the matched layer; but, when there are turbulent stresses in the flow, Fourier components travelling faster or slower than the mean velocity can lead to gradients in shear stress.

The question this paper addresses is whether the interaction of the lateral velocity components with the mean flow accounts for most of the shear stress gradient, or whether the lateral velocity fluctuations interact strongly with the other turbulent fluctuations present in the flow. This can be tested in a mixing layer by measuring the convection velocity of the Fourier components of the shear stress, and comparing the velocity of the most energetic components with the local mean.

The interaction of the Fourier components of the lateral velocity with the other turbulent quantities can be examined by Fourier transforming the momentum equation and forming a product with the lateral velocity components. Such an exercise could show the role of the nonlinear terms in the maintenance of shear stress, if they were evaluated from spectral measurements. Measurement of all the components involved was beyond our patience, but some simple deductions can be made from the spectral components that were measured in the mixing layer.

2. Apparatus and co-ordinates

The two-dimensional mixing layer was generated in the apparatus used by Wygnanski & Fiedler (1970), where the flow (sometimes called a half-jet) was allowed to entrain ambient air along one of its boundaries, the other three being solid surfaces as shown in figure 1. A trip wire, 1 cm upstream of the nozzle exit, ensured a turbulent boundary layer on the nozzle wall.

The longitudinal velocities were sensed with single hot-wire probes and the lateral velocities with X-wires. Four DISA 55D01 anemometers and 55D10 linearizers were required to measure correlations of lateral velocities. The sum

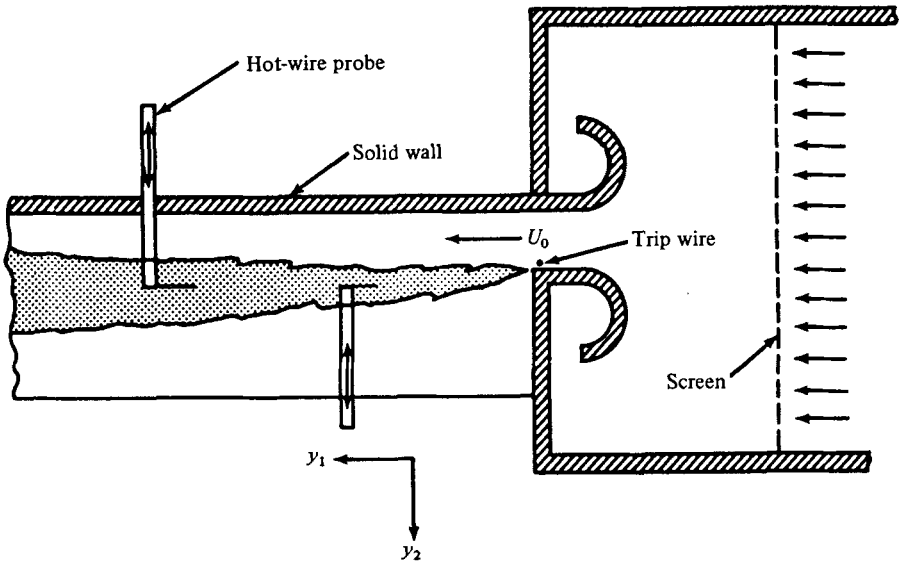

FIGURE 1. Schematic of two-dimensional mixing layer and two hot-wire probes.

and difference of X-wire outputs were produced with the aid of Philbrick components.

Fourier transformations of the fluctuating quantities were produced on an IBM 360-44 computer. The signals from two measuring stations were digitized with an 11 bit word length by an IBM 1827 analog-to-digital converter at the rate of 3500 samples per second per channel. A 'fast Fourier transform of these signals in bands 3·5 c/s wide gave a description of the energy above 1·7 c/s with a folding frequency of 1700 c/s. Because the two channels were sampled sequentially, the time delay between signals was equivalent to a phase shift. This delay was 56 μs, giving rise to phase shift of 0·06 rad at the highest frequency used (about 0·1 of the folding frequency, to ensure no aliasing problem). A satisfactory statistical certainty was obtained with 150–200 ensembles.

The spacing between the measuring stations was varied, to produce filtered correlations, which were transformed for each frequency band to produce a wavenumber frequency spectrum. The smallest spacing was set by problems of probe interference; and this was most severe in measurements using an X-wire upstream of another wire. At the smallest separation used, the maximum variation in spectral bands due to the interference to the flow from the upstream wire was about 5%. At the largest separation, the distance between the probes was 60 cm. The lowest-frequency band computed was 17 c/s, which gives a percentage bandwidth (in frequency) of $\pm 0{\cdot}1$ of the centre frequency. Higher frequencies had a lower percentage bandwidth to ensure that the error in computing the correlation, as a result of finite bandwidth, was less than 10% for 1·25 cycles (in space) of the filtered correlation.

The co-ordinate system y_i adopted had y_1 in the downstream direction, and y_2 in the lateral direction containing the variation of mean velocity. The lateral co-ordinate was made non-dimensional by y_1, where y_1 was zero at the virtual

origin of the mixing layer, 1·9 cm upstream of the nozzle lip (from Wygnanski & Fiedler 1970). This variable η (i.e. y_2/y_1) had its origin at the point where the mean velocity was half the exit velocity U_0. Fluctuations about the mean velocity U_i are written as u_i.

3. Definition of spectra

The velocities $u_i(t)$ sensed by the hot-wire probes were transformed into Fourier frequency modes $Z_i(\omega)\,d\omega$, defined by

$$u_i(t) = \int_{-\infty}^{\infty} \exp(+i\omega t)\, Z_i(\omega)\, d\omega. \tag{1}$$†

Because the transformation was digital, the estimates of $Z_i(\omega)$ are available only at discrete values of ω; but in this discussion we shall treat $Z_1(\omega)$ as if it were continuous in ω.

Transforms of velocity sensed at two positions, separated in space by distance $\mathbf{r}$, were multiplied together, i.e.

$$Z_i(\omega, \mathbf{y})\, Z_j^*(\omega, \mathbf{y}+\mathbf{r}),$$

to form complex numbers, which were then averaged over a number of realizations, to produce

$$\overline{Z_i(\omega, \mathbf{y})\, Z_j^*(\omega, \mathbf{y}+\mathbf{r})\, d\omega}.$$

This quantity can be shown to equal the transform of the velocity covariance

$$\frac{1}{2\pi}\int_{-\infty}^{\infty} \mathscr{R}_{ij}(t, \mathbf{y}, \mathbf{r}) \exp(-i\omega t)\, dt.$$

(See e.g. Lumley & Panofsky 1964.) Here,

$$\mathscr{R}_{ij}(t, \mathbf{y}, \mathbf{r}) = \overline{u_i(t', \mathbf{y})\, u_j(t'+t, \mathbf{y}+\mathbf{r})};$$

and we are prepared to assume $\mathscr{R}_{ij}$ is stationary in time. When $\mathbf{r} = 0$, this spectral product reduces to the usual autospectrum, i.e.

$$\Omega_{ij}(\omega, \mathbf{y}) = \overline{Z_i(\omega, \mathbf{y})\, Z_j^*(\omega, \mathbf{y})\, d\omega}.$$

Since $\mathscr{R}_{ij}(t, \mathbf{y}, \mathbf{r})$ is real, the real part of $\overline{Z_i(\omega, \mathbf{y})\, Z_j^*(\omega, \mathbf{y}+\mathbf{r})\, d\omega}$ is even in ω, and the imaginary part is odd. In order to perform spatial transformations, a coefficient was calculated from the spectral coefficients, i.e.

$$C_{ij}(\omega, \mathbf{y}, \mathbf{r}) = \frac{\overline{Z_i(\omega, \mathbf{y})\, Z_j^*(\omega, \mathbf{y}+\mathbf{r})}}{[Z_i(\omega, \mathbf{y})\, Z_i^*(\omega, \mathbf{y})\, Z_j(\omega, \mathbf{y}+\mathbf{r})\, Z_j^*(\omega, \mathbf{y}+\mathbf{r})]^{\frac{1}{2}}}. \tag{2}$$

Repeated subscripts do not imply summation in this paper. This filtered space correlation, which appears to have been first considered by Wills (1964), is bounded by ± 1.

† $Z_i(\omega)$ does not in general have derivatives.

Wavenumber transformations of the above coefficient were made numerically, e.g.

$$\left.\begin{aligned}\mathscr{M}_{ij}(\mathbf{y}, k_1, \omega) &= \frac{\Omega_{ii}^{\frac{1}{2}}(\omega, \mathbf{y})\,\Omega_{jj}^{\frac{1}{2}}(\omega, \mathbf{y})}{\pi}\int_0^\infty C_{ij}(\omega, \mathbf{y}, r_1)\exp(ik_1 r_1)\,dr_1,\\ \mathscr{M}_{ij}(\mathbf{y}, k_2, \omega) &= \frac{\Omega_{ii}^{\frac{1}{2}}(\omega, \mathbf{y})\,\Omega_{jj}^{\frac{1}{2}}(\omega, \mathbf{y})}{\pi}\int_0^\infty C_{ij}(\omega, \mathbf{y}, r_2)\exp(ik_2 r_2)\,dr_2.\end{aligned}\right\} \tag{3}$$

If we assume C_{ij} is even in r, and that the flow field is homogeneous in spectral bands (i.e. $\overline{Z_j(\omega, \mathbf{y})\,Z_j^*(\omega, \mathbf{y})}$ is independent of $\mathbf{y}$), the above transform is equivalent to the more usual definition of spectra

$$\mathscr{M}_{ij}(k_1, \omega) = \left(\frac{1}{2\pi}\right)^2 \int_{-\infty}^{\infty} \mathscr{R}(t, \mathbf{y}, r_1)\exp[i(k_1 r_1 - \omega t)]\,dt\,dr_1.$$

Since the real part of $\overline{Z_i(\omega, \mathbf{y})\,Z_j^*(\omega, \mathbf{y}+\mathbf{r})\,d\omega}$ is even in ω, and the imaginary part odd in ω, it follows from (2) that C_{ij} also has this property, and from (3) that

$$\mathscr{M}_{ij}(k_m, \omega) = \mathscr{M}_{ij}(-k_m, -\omega).$$

In a two-dimensional mixing layer, the above two assumptions are true for separations in the direction where the properties are uniform, but they must be treated cautiously for streamwise separations (and also for lateral directions, not considered in this paper). We assumed that $C_{ij}(\omega, \mathbf{y}, \mathbf{r})$ is invariant to reflexion about the r axis, and that Ω_{jj} is invariant to translation (over regions about $\mathbf{y}$ where $C_{ij}(\omega, \mathbf{y}, \mathbf{r})$ is not zero). For streamwise displacements, $\Omega_{jj}(\omega, \mathbf{y})$ varies appreciably, since it scales on the distance downstream: but fortunately the value $\Omega_{jj}(\omega, \mathbf{y})$, which must be equated to $\Omega_{jj}(\omega, \mathbf{y}+\mathbf{r})$ for the usual definition of a spectrum, does represent something like the mean value of $\Omega_{jj}(\omega, \mathbf{y}+\mathbf{r})$ over both positive and negative values of displacement. The errors induced by the above assumptions will be most pronounced for the low-frequency low-wavenumber portion of the spectra, where the integration extends to larger separations.

We have available at least two options in actually transforming the C_{ij} functions in (3). We can transform the actual estimates of C_{ij} that were computed for a finite number of $\mathbf{r}$ displacements, or we can fit a curve to C_{ij} and transform this continuous function. The latter approach allows us to make an estimate of the spectrum at low wavenumbers which, although only as good as our curve-fitting model extrapolated beyond the data, does provide some estimate of the spectrum at low wavenumbers. This approach was adopted here.

The function chosen to fit the modulus of the complex C_{ij} was

$$|C_{ij}(r_l, \omega)| = |C_{ij}(0, \omega)|\exp -(a|r_l|^n), \tag{4}$$

while the phase angle of $C_{ij}(r_l, \omega)$, i.e.

$$\theta_{ij} = \tan^{-1}\frac{\mathrm{Im}\,[C_{ij}(r_l, \omega)]}{\mathrm{Re}\,[C_{ij}(r_l, \omega)]}, \tag{5}$$

was fitted by a function $c + br_l$. Thus we used

$$C_{ij}(r_l, \omega) = |C_{ij}(0, \omega)|\exp -(a|r_l|^n)\exp[i(c + br_l)]. \tag{6}$$

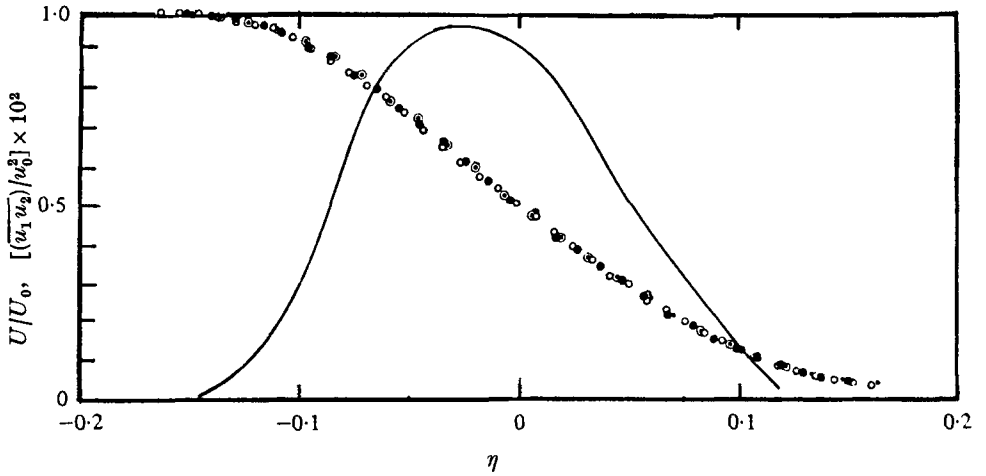

FIGURE 2. The mean velocity profile and the shear stress profile calculated from the velocity profile, reproduced from Wygnanski & Fiedler (1970). ———, shear stress.

y_1(in.)	23·1	19·23	15·275
	○	●	⊙

The degree of success of fitting the measured C_{ij} by a four-parameter curve, a, b, c, n, is shown in later sections. In the actual fitting routine, once the coherence of the data dropped below 4% (i.e. $|C_{ij}| < 0{\cdot}2$) twice, $C_{ij}(\mathbf{r}, \omega)$ was considered to be of low statistical reliability, and ignored.

4. Results

4.1. *Exit conditions*

The trip wire on the upstream wall of the mixing layer produced a turbulent boundary layer with a displacement thickness of 0·8 cm. The typical free-stream turbulence level at the exit plane was less than 0·3% for both the lateral ($\widetilde{u_2}/U_0$) and the longitudinal fluctuations.

Wygnanski & Fiedler (1970) measured many of the properties of this self-preserving mixing layer, and we have reproduced their mean velocity profiles in figure 2. The present mixing layer spreads more rapidly than that of the round jet studied by Bradshaw, Ferriss & Johnson (1964), with which frequent comparisons are made, and the two-dimensional mixing layer of Liepmann & Laufer (1947). In the case of two-dimensional mixing layers, the changed rate of spread was attributed by Batt, Kubota & Laufer (1970) to the differential initial conditions.

4.2. *Longitudinal velocity spectra*

The conventional frequency spectrum of the longitudinal velocity fluctuations is defined as

$$\phi_{11}(\omega) = \frac{2U_0}{y_1 \overline{u_1^2}} \overline{Z_1(\omega, \mathbf{y}) Z_1^*(\omega, \mathbf{y})}\, d\omega.$$

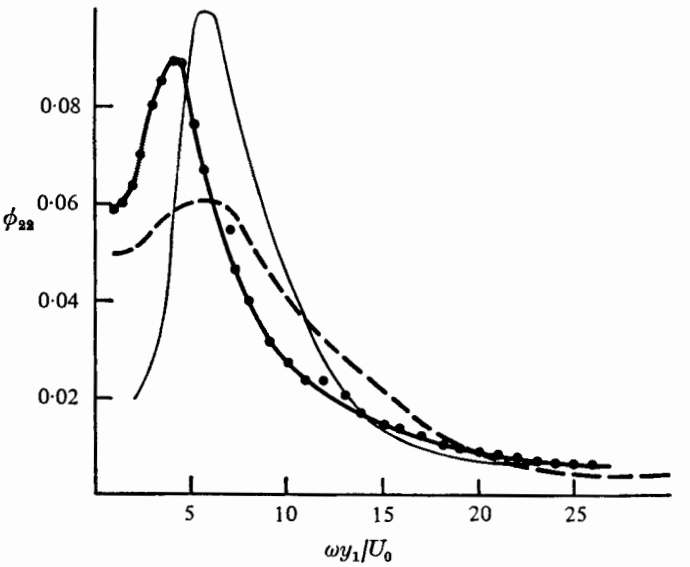

FIGURE 3. The frequency spectrum of the longitudinal velocity fluctuations (–·–·–) compared with Bradshaw *et al.* (– – – –), together with the spectrum of the lateral velocity fluctuations (———). $y_1 = 27$ cm, $U_0 = 12$ m s^{-1}, $\eta = -0{\cdot}075$.

This spectrum is real, as is any complex number multiplied by its conjugate, and is even in ω, since

$$Z_i^*(\omega) = Z_i(-\omega)$$

from the definition of (1). The factor $2U_0/y_1\overline{u_1^2}$ is introduced to give $\phi_{11}(\omega)$ the property

$$\int_0^\infty \phi_{11}(\omega)\, d\omega\, y_1/U_0 = 1.$$

The spectrum on the high-speed side of the mixing layer, 27 cm downstream of the virtual origin, is shown in figure 3 and compared with the results obtained by Bradshaw *et al.* (1964) in a round jet. The values of η are defined as in §2, for all results.

Since the widths of the mixing layers are different at the same y_1, it is not surprising that the non-dimensional frequency $\omega y_1/U_0$ is not a good scaling parameter. A better collapse of the data from the two different experiments would have been achieved by using some characteristic local width of the mixing layer in place of y_1, possibly like that proposed by Jones (1968).

As well as the usual autospectrum, we measured, on the high-velocity side of the mixing layer, the spectral product $\overline{Z_1(\omega, \mathrm{y})\, Z_1^*(\omega, \mathrm{y}+r_1)\, d\omega}$, and formed the filtered correlation $C_{11}(\omega, r_1)$ of (2), which is presented in figure 4 as the modulus of $C_{11}(\omega, r_1)$ and the phase angle θ_{11}. The modulus of $C_{11}(\omega, r_1)$ is the square root of the coherence and bounded by 1 and 0. The coefficient at the origin (i.e. $C_{11}(\omega, 0)$) is unity, and there is no inherent difficulty fitting the modulus of C_{11} with the function $\exp(-ar_1^n)$ of (4) by a least-squares technique. The fitted curve

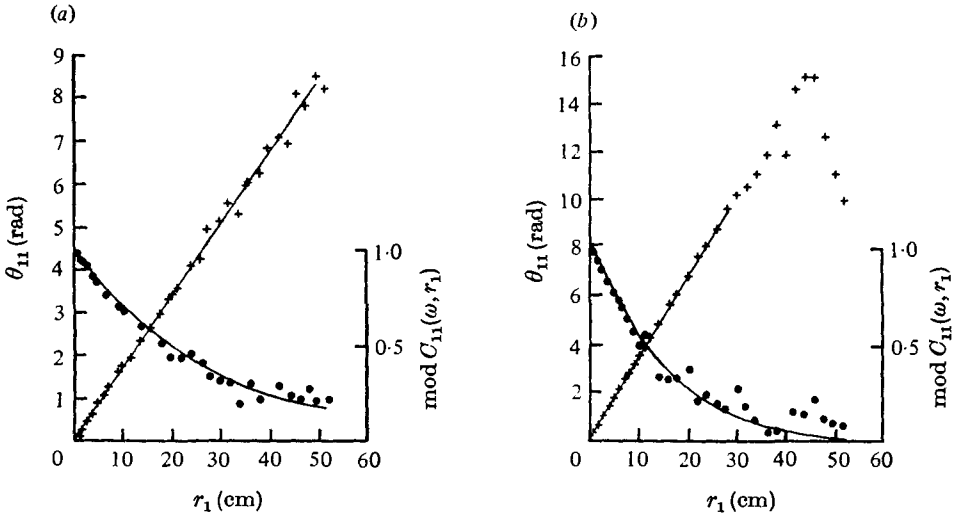

FIGURE 4. Filtered correlations of longitudinal velocity fluctuations, showing the square root of coherence and the phase angle. +, data; ———, fitted function. $y_1 = 27$ cm, $U_0 = 12\,\mathrm{m\,s^{-1}}$. $\omega y_1/U_0$: (*a*) 3; (*b*) 7.

is shown as a solid line in figure 4. Since the turbulence is convected in the r_1 direction by the mean velocity, the signal at r_1 lags the signal at $r_1 = 0$, so that the phase angle, as defined in (5), becomes increasingly positive with r_1. The phase angle is only defined $\pm 2\pi$; thus, the computer program has added the appropriate number of cycles, in order to fit $\theta_{11}(\omega)$ with the function $c + br_1$. The fitting was accomplished by a least-squares technique, which weighted the data near $r_1 = 0$ in order to determine c, before fitting all the data for values of r_1 less than the separation at which the coherency had dropped below 4% at two previous positions. Since $C_{11}(\omega, r)$ at $r = 0$ is real, the phase angle at $r = 0$ must be zero and in turn $c = 0$.

Thus the coefficient C_{11} was fitted by $\exp(-ar_1^n)\exp(ibr_1)$, assumed even in r_1, assumed homogeneous in spectral bands, then transformed to produce an approximation to the spectrum $M_{11}(k_1, \omega)$ defined in the appendix.

We made no test of the evenness of $C_{11}(\omega, r_1)$; but it does reach its maximum value of unity at the origin. The modulus of C_{11} most likely decays more rapidly in the $-r_1$ direction where, because of lack of homogeneity, characteristic scales of the turbulence are smaller.

A number of complex transforms of $C_{11}(\omega, r_1)$ at constant ω are shown in figure 5; and these are analogous to the Fourier cosine transform presented by Wills (1964), except that we present spectral densities of only positive wavenumbers, rather than the sum of both positive and negative. These curves have the property

$$\int_0^\infty \int_{-\infty}^\infty M_{11}(k_1, \omega)\, dk_1 y_1 \frac{d\omega y_1}{U_0} = 1;$$

they are $\mathcal{M}_{11}(k_1, \omega)$ of (3), multiplied by $2U_0/y_1^2\overline{u_1^2}$. Contours of equal $M_{11}(k_1, \omega)$ have been drawn in figure 6; they show the concentration of energy along a line

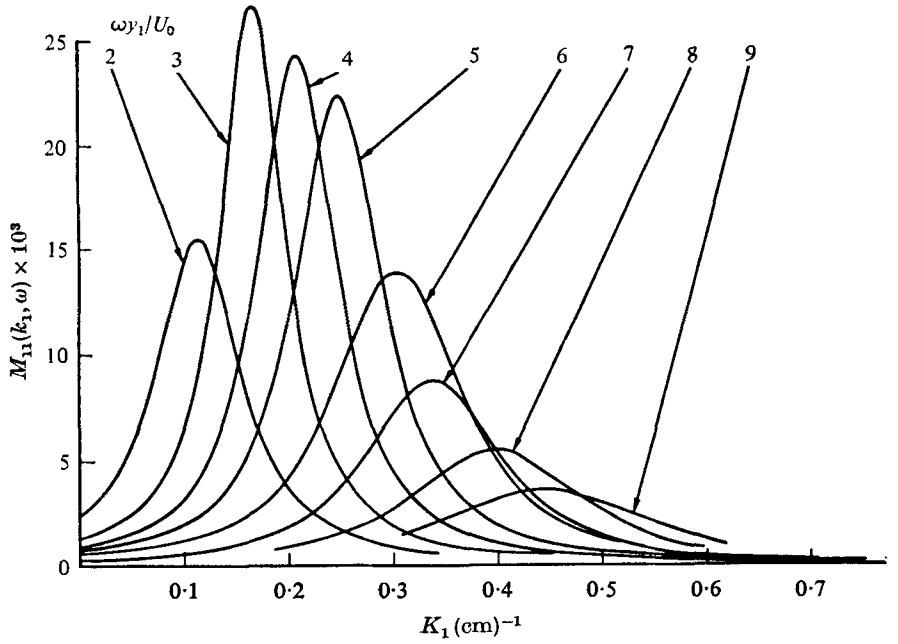

FIGURE 5. Wavenumber frequency spectra of velocity fluctuations at $y_1 = 27$ cm, $\eta = -0{\cdot}075$, $U_0 = 12\,\mathrm{m\,s^{-1}}$.

approximately $\omega y_1/U_0 = 0{\cdot}72\,k_1 y_1$, signifying convection in the downstream direction. The extrapolation from the data by the fitted curve provides the information from which the spectrum at zero wavenumber is calculated.

The spectrum in figure 6 can be compared with Will's wavenumber frequency spectrum in a round jet, published by Bradshaw & Ferriss (1965). The frequency spectrum in this round jet is less sharply peaked than the present mixing layer. (See figure 3.) Hence it is not surprising that Wills' k_1, ω spectrum also has a weaker peak. The present contours are less elongated along the k_1, ω convection line, although the peak does occur at the same value of ω/k_1 (i.e. $0{\cdot}72\,U_0$).

Filtered correlations with displacements in the r_3 direction were measured, and fitted with (6). As in the previous case, c must be zero; but now we find that frequency components are in phase for displacements in the r_3 direction (as long as there is significant coherence), leading to a value of b close to zero. The k_3 transform becomes

$$\phi_{11}(\omega)\,(\pi y_1)^{-1} \int_0^\infty \exp(-a r_3^n) \exp(i k_3 r_3)\, dr_3. \tag{7}$$

To the extent that the flow is exactly two-dimensional, quantities are homogeneous and even in r_3, so that (7) is exactly equal to $M_{11}(k_3, \omega)$ defined in table 1. $M_{11}(k_3, \omega)$ spectral densities are shown in figure 7 for positive values of k_3 only, because they are symmetrical in k_3. The filtered correlations showed no tendency to have negative loops, so the maximum value of the spectrum occurs at $k_3 = 0$, rather than at some positive value as in the k_1, ω spectrum.

For frequencies above and below $\omega y_1/U_0 = 4$, the constant-frequency spectra

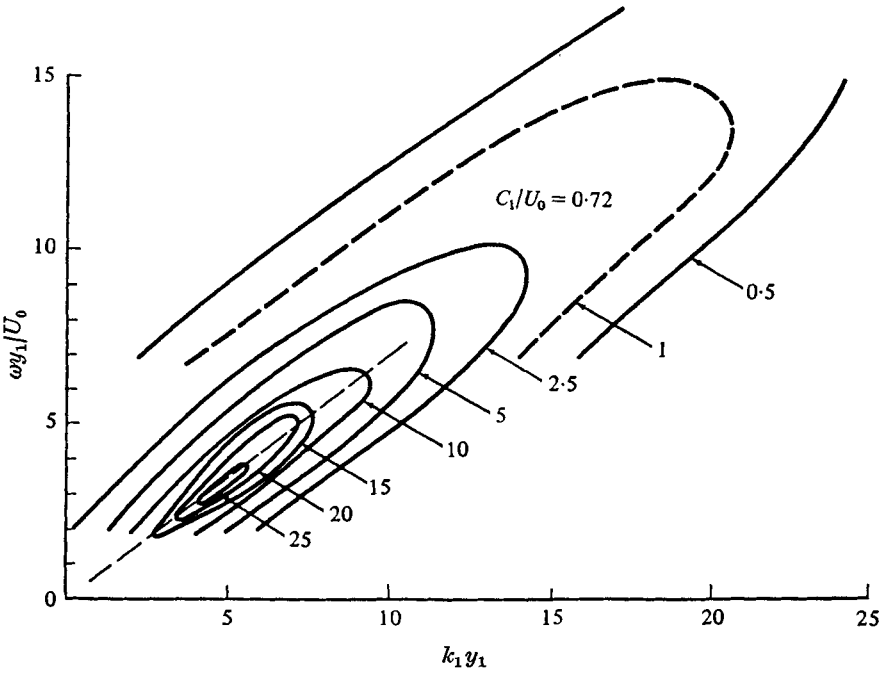

FIGURE 6. Contours of wavenumber frequency spectra $M_{11}(k_1, \omega) \times 10^3$ at $y_1 = 27$ cm, $\eta = -0{\cdot}075$, $U_0 = 12\,\mathrm{m\,s^{-1}}$.

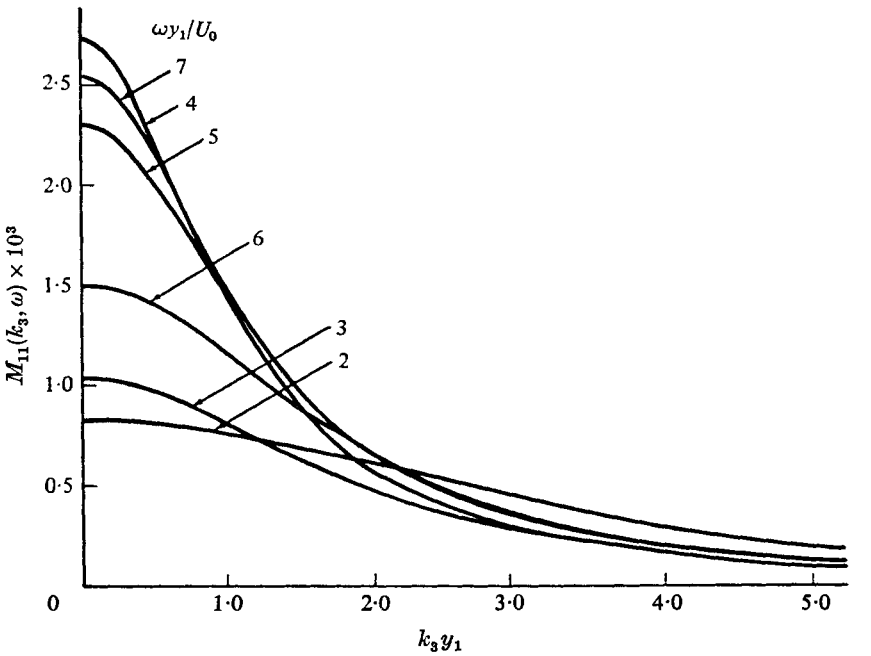

FIGURE 7. Wavenumber frequency spectra of velocity fluctuations at $y_1 = 27$ cm, $\eta = -0{\cdot}075$, $U_0 = 12\,\mathrm{m\,s^{-1}}$.

in figure 7 have greater concentrations of energy at high wavenumbers than the more sharply peaked spectrum at $\omega y_1/U_0 = 4$. This implies that the eddies of the highest and lowest frequencies are of smaller lateral extent than those of intermediate frequencies. This strikes the author as peculiar; and it was not observed in e.g. the k_3, ω spectrum, for the pressure fluctuations beneath a turbulent boundary layer, presented by Wills (1971). None of the filtered correlations $C_{11}(\omega, r_3)$ exhibit significant coherence at values of r_3 greater than the width (in the y_2 direction) of the mixing layer.

The two spectra discussed above were functions of two dimensions: frequency, and a wavenumber in the direction of one of the co-ordinate axes. In order to compute in a similar manner a three-dimensional spectrum, say $\hat{M}_{11}(k_1, k_3, \omega)$, it would be necessary to make measurements at a large number of displacements in the r_1, r_3 plane. While this is possible, it would be convenient to construct the three-dimensional spectrum from the simpler $M_{11}(k_1, \omega)$ and $M_{11}(k_3, \omega)$ spectra, reducing the number of measurements involved.

The filtered correlation with displacements in two directions, $\hat{C}_{11}(r_1, r_3, \omega)$, was assumed separable with respect to r_1 and r_3, i.e.

$$\hat{C}_{11}(r_1, r_3, \omega) = C_{11}(r_1, \omega)\, C_{11}(r_3, \omega). \tag{8}$$

This separation was suggested by Jones (1969), for use in evaluating Lighthill's aerodynamic noise integral. From (8) and the definitions in table 1, it follows that

$$\hat{M}_{11}(k_1, k_3, \omega) = M_{11}(k_1, \omega)\, M_{11}(k_3, \omega)/\phi(\omega); \tag{9}$$

and the spectrum of (9) reduces exactly to the simpler two-dimensional spectrum, e.g.

$$M_{11}(k_3, \omega) \equiv \int_{-\infty}^{\infty} \hat{M}_{11}(k_1, k_3, \omega)\, dk_1 y_1.$$

In the space-time domain, the separation in (8) is equivalent to a convolution (with respect to time) of the Fourier transforms of $C_{11}(r_1, \omega)$ and $C_{11}(r_3, \omega)$.

The separation used in (8) is equivalent to assuming that the distribution of energy in the k_3 wavenumber for each k_1 is the same as that of the distribution integrated over all k_1 (i.e. $M_{11}(k_3, \omega)$. Wills (1971) discussed the separation of wavenumber frequency spectra for the pressure fluctuations beneath a turbulent boundary layer. He chose a somewhat analogous separation; but, because he wanted a two-dimensional spectrum in terms of k_1 and k_3, he integrated over ω.

The $\hat{M}_{11}(k_1, k_3, \omega)$ spectra is shown for a fixed value of frequency in figure 8, while it is shown for a higher frequency in figure 9, for only positive values of k_3 (since it is symmetrical). The contours in these two figures are elliptical and, because they encompass a narrow band of frequencies, the contours are centred on a value of k_1 that is set by the convection of these frequencies past a fixed observer.

The separation of filtered correlations in (8) used to obtain the three-dimensional spectrum leads to exact two-dimensional spectra along the wavenumber axes. It is desirable to test how well the three-dimensional spectrum reduces to a two-dimensional spectrum for wavenumbers not on the axes.

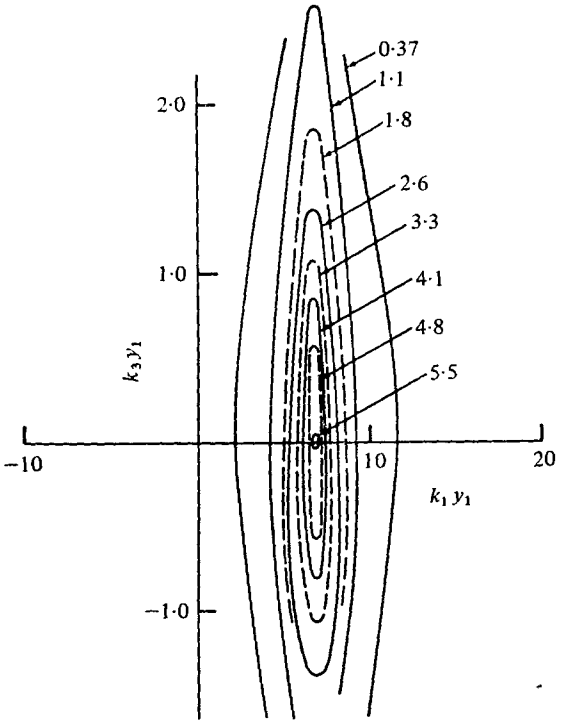

FIGURE 8. Contours of wavenumber frequency spectrum of velocity fluctuations $\hat{M}_{11}$ $(k_1, k_3, \omega) \times 10^4$ at a constant frequency $y_1 = 27$ cm, $\eta = -0{\cdot}075$, $U_0 = 12\,\mathrm{m\,s^{-1}}$. $\omega y_1/U_0 = 5$. This spectrum computed using separation assumption.

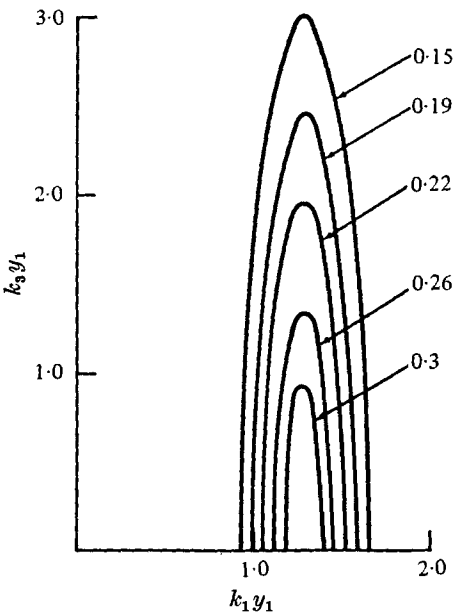

FIGURE 9. Contours of wavenumber frequency spectrum of velocity fluctuations $\hat{M}_{11}$ $(k_1, k_3, \omega) \times 10^4$ at a constant frequency. Spectrum is symmetrical about $k_3 = 0$, $y_1 = 27$ cm, $\eta = -0{\cdot}075$, $U_0 = 12\,\mathrm{m\,s^{-1}}$ $\omega y_1/U_0 = 10$. This spectrum computed using separation assumption.

A spectrum that is a function of κ_1, being a wavenumber in the k_1, k_3 plane, is obtained from $\hat{M}_{11}(k_1, k_2, \omega)$ by integrating in a direction perpendicular to κ_1. The steps involved can be seen by considering the inverse transformation,

$$\mathscr{R}_{ij}(t, \mathbf{y}+\mathbf{r}') = \int_0^\infty \int_{-\infty}^\infty \mathscr{M}_{ij}(\mathbf{y}, \mathbf{k}', \omega) \exp\left[-i(\mathbf{k}'\mathbf{r}' - \omega t)\right] d\omega d\mathbf{k}. \tag{10}$$

$\mathbf{r}'$ and $\mathbf{k}'$ are two-dimensional vectors. Let Γ be a displacement at angle α to the r_1 axis, and κ_1 and κ_3 are defined below, i.e.

$$\begin{aligned} r_1 &= \Gamma\cos\alpha, \quad & k_1 &= \kappa_1\cos\alpha, \quad & k_1 &= k_3\sin\alpha, \\ r_3 &= \Gamma\sin\alpha, \quad & k_3 &= \kappa_1\sin\alpha, \quad & k_3 &= \kappa_3\cos\alpha. \end{aligned}$$

Then substitution in (10) leads to

$$\mathscr{R}_{ij}(t, \mathbf{y}, \Gamma, \alpha) = \int_{-\infty}^\infty \int_{-\infty}^\infty \int_0^\infty \mathscr{M}_{ij}(\mathbf{y}, k_1, k_2, \omega) \exp -i(\kappa_1\Gamma - \omega t)\cos^2\alpha\, d\omega\, d\kappa_1 d\kappa_3.$$

The transform of both sides of this expression leads to

$$\frac{1}{2\pi^2}\int_{-\infty}^\infty \int_{-\infty}^\infty \mathscr{R}_{ij}(t, \mathbf{y}, \Gamma, \alpha) \exp\left[i(\Gamma\kappa_1 - \omega t)\right] d\Gamma dt = \int_{-\infty}^\infty \mathscr{M}_{ij}(\mathbf{y}, k_1, k_3, \omega)\cos^2\alpha\, d\kappa_3. \tag{11}$$

The integral on the right-hand side of (11) is our definition of the two-dimensional spectrum $M_{ij}(\mathbf{y}, \kappa_1, \omega)$. Thus, $M_{11}(\mathbf{y}, \kappa_1, \omega)$ was computed from the $\mathscr{M}(\mathbf{y}, k_1, k_3, \omega)$ spectrum using (11). The results are shown in figures 10 and 11 for $\alpha = \tan^{-1} 0{\cdot}2$; they are normalized so that

$$\int_0^\infty \int_{-\infty}^\infty M_{11}(\mathbf{y}, \kappa_1, \omega)\, d\kappa_1 y_1 d\omega y_1/U_0 = 1.$$

Also shown in figure 10 is $M_{11}(\mathbf{y}, \kappa_1, \omega)$, calculated from directly measured values of C_{11} at a number of values of Γ. As before, the filtered correlations are fitted by (6), then transformed.

The computed three-dimensional spectrum reduces to a two-dimensional spectrum that is only order three quarters of the measured spectrum, although the peak in the energy occurs at the same frequency. While this obviously reflects the failure of the simplifying separation assumption of (8), the correspondence between the measured and computed spectra is heartening; it suggests that the separation with respect to wavenumbers may be an acceptable procedure for approximate calculations. Evaluation of a structure constant in §5 is one such calculation.

4.3. *Lateral velocity spectra*

The lateral fluctuations of velocity across the mean velocity gradient play a role in the maintenance of shear stress, so we have measured, on the high-velocity side of the mixing layer, the spectrum of these fluctuations at the same position as the previous longitudinal velocity spectra. The conventional autospectrum, shown in figure 3, exhibits the characteristic peak observed by Bradshaw *et al.* (1964) on the inner edge of their mixing layer. Contours of $M_{22}(k_1, \omega)$ are shown in

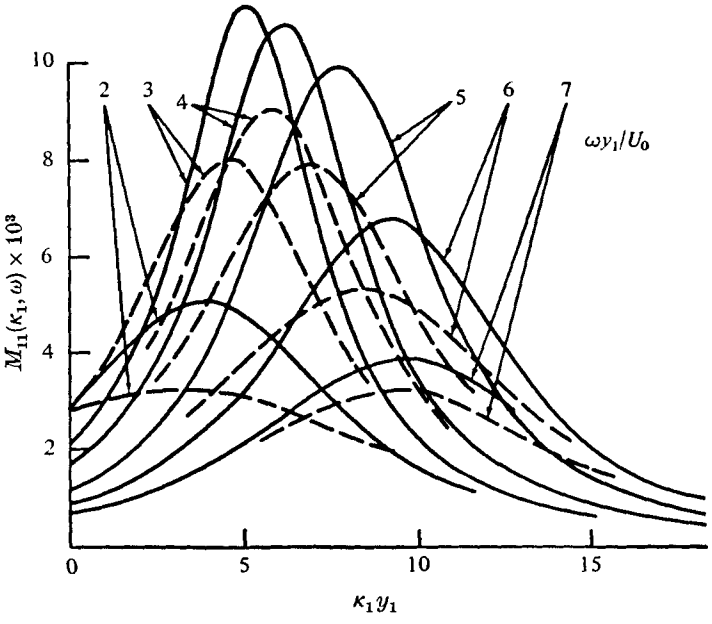

FIGURE 10. Comparison between measured κ_1, ω spectrum and spectrum computed from $\hat{M}_{11}(k_1, k_3, \omega)$ spectrum. $\kappa_1 = k_1 \cos\alpha + k_3 \sin\alpha$, $y_1 = 27$ cm, $\eta = -0{\cdot}075$, $U_0 = 12\,\mathrm{m\,s^{-1}}$. ———, measured; – – – –, computed.

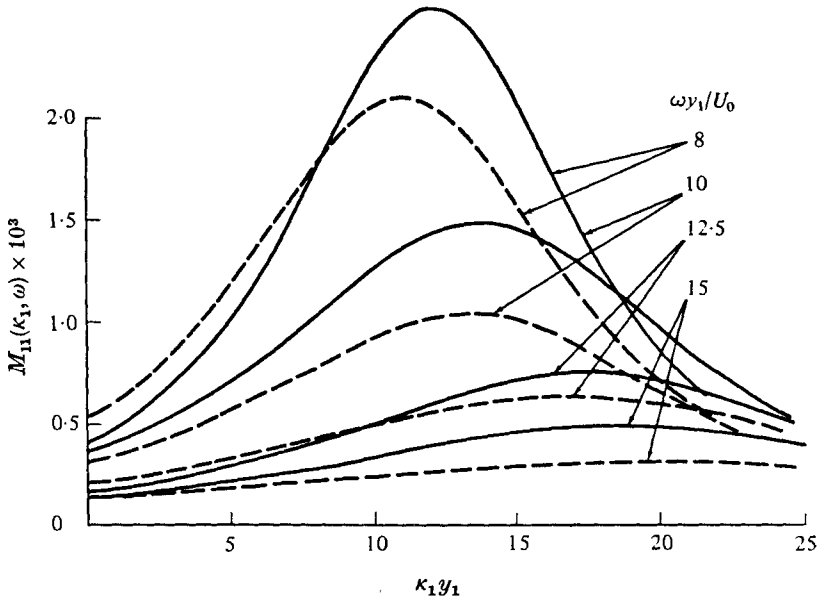

FIGURE 11. Comparison between measured κ_1, ω spectrum and spectrum computed from $\hat{M}_{11}(k_1, k_3, \omega)$ spectrum. $\kappa_1 = k_1 \cos\alpha + k_3 \sin\alpha$, $y_1 = 27$ cm, $\eta = -0{\cdot}075$, $U_0 = 12\,\mathrm{m\,s^{-1}}$. ———, measured; – – – –, computed.

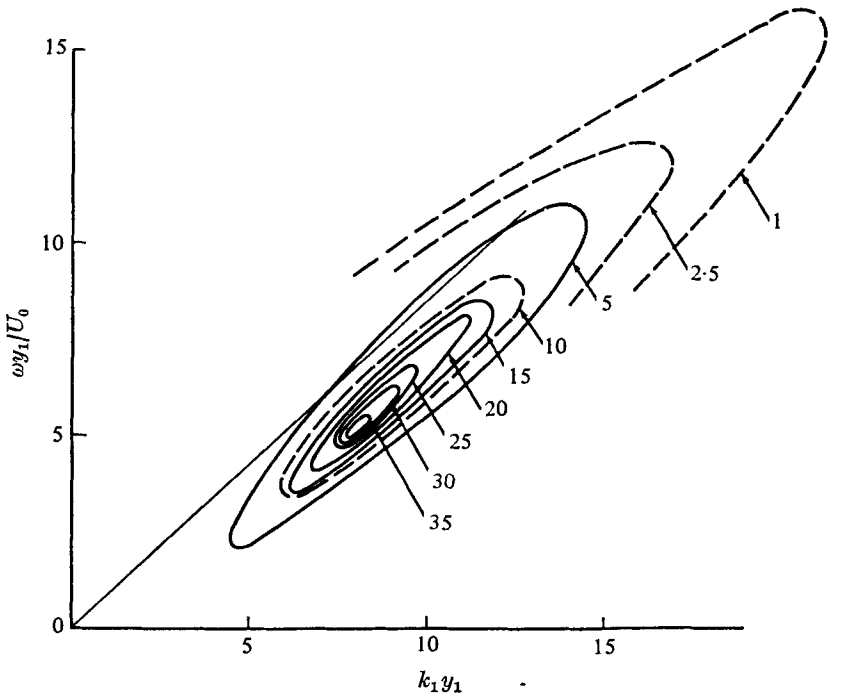

FIGURE 12. Contours of the wavenumbers frequency spectrum of lateral velocity fluctuations $M_{22}(k_1, \omega) \times 10^3$. $y_1 = 27$ cm, $\eta = -0{\cdot}075$, $U_0 = 12\,\mathrm{m\,s^{-1}}$.

figure 12, and they exhibit a sharp peak centred at $\omega y_1/U_0 = 5$ and $k_1 y_1 = 8$, higher values than those for the peak in the $M_{11}(k_1, \omega)$ spectrum.

The spectrum for the lateral wavenumber $M_{22}(k_3, \omega)$ shown in figure 13 has a markedly greater proportion of its energy in high wavenumbers than the $M_{11}(k_3, \omega)$ spectrum. Bradshaw *et al.* (1964) observed that the correlation of u_2 fluctuations with lateral displacements (i.e. r_3) was greater than the correlation of u_1 fluctuations, and this is consistent with observed filtered correlations that were used to generate the wavenumber frequency spectra. These two spectra of lateral fluctuations are used in §5 to evaluate the structure constant proposed by Phillips (1969).

4.4. *Shear stress*

The mean shear stress $\overline{u_1 u_2}$ is central to a turbulent shear flow, as it both diffuses momentum and contributes to the generation of turbulence. Its profile in the mixing layer has been reproduced from Wygnanski & Fiedler (1970) in figure 3. The mean shear stress is related to the product of $Z_1(\omega)$ and $Z_2(\omega)$ by

$$\overline{u_1 u_2}(\mathbf{y}) = \int_{-\infty}^{\infty} \Omega_{12}(\omega, \mathbf{y})\, d\omega. \tag{12}$$

The imaginary part of $\Omega_{12}(\omega, \mathbf{y})$, unlike the imaginary parts of $\Omega_{11}(\omega, \mathbf{y})$ or $\Omega_{22}(\omega, y)$, is not necessarily zero, although, when it is integrated over all ω,

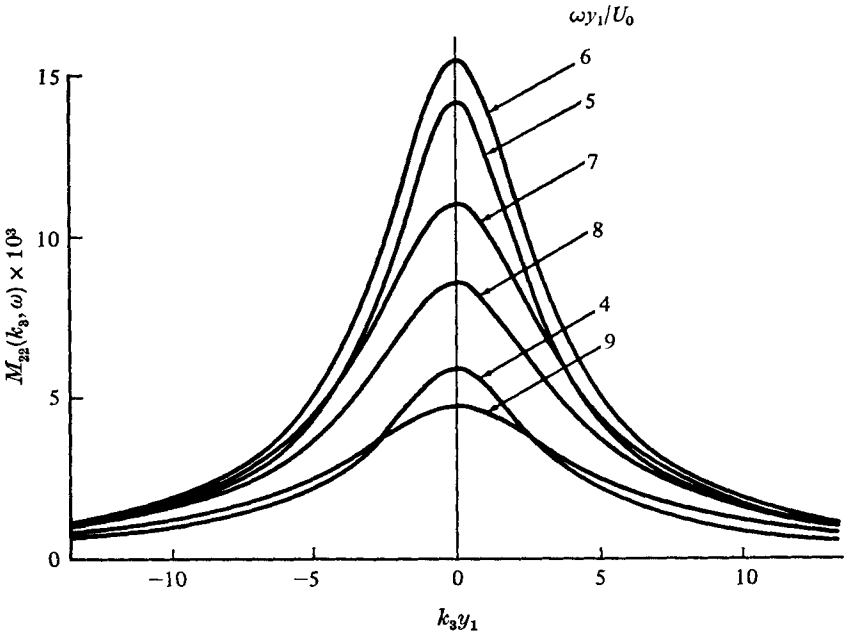

FIGURE 13. Lateral velocity spectra $M_{22}(k_3, \omega)$ at constant frequency. $y_1 = 27$ cm, $\eta = 0{\cdot}075$, $U_0 - 12\,\mathrm{m\,s^{-1}}$.

the resultant integral must equal zero (because $\overline{u_1 u_2}$ is real). We shall call the real part of the $\Omega_{12}(\omega, y)$ spectrum $\Phi_{12}(\omega)$, when it is normalized so that

$$\int_0^\infty \Phi_{12}(\omega) \frac{d\omega y_1}{U_0} = \frac{\overline{u_1 u_2}}{U_0^2}. \tag{13}$$

This co-spectrum has been measured at a number of positions on the high-velocity side of the mixing layer, and is shown in figure 14. All spectra exhibit a sharp peak near $\omega y_1/U_0 = 5$, with the lateral gradient of $\overline{u_1 u_2}$ in figure 3 coming from a more or less uniform increase in all frequencies. The $\Phi_{12}(\omega)$ spectrum gives an indication of the characteristic frequency of the turbulent energy production, because $\overline{u_1 u_2}\ \partial U/\partial y_2$ is the dominant production term in the energy equation. (Cf. Wygnanski & Fiedler 1970.) The fitted coefficient $C_{12}(\omega, \mathrm{y})$ has a real part, which depicts those components that contribute to the shear stress, and an imaginary part, which describes those components of the lateral and longitudinal velocity fluctuations that are coherent but 90 degrees out of phase. As we noted in § 3, the real part of $C_{ij}(\omega, \mathrm{y}, 0)$ is even in ω, so we have presented $C_{12}(\omega, \mathrm{y}, 0)$ in figure 15 for positive values of ω only. Here the shear stress coefficient at a number of positions across the mixing layer is compared with the measurements of Bradshaw *et al.* (1964). In the two-dimensional mixing layer the coefficients, while having the same maximum value, appear to be smaller at higher frequencies than do the coefficients for the round jet. This is similar to the difference between the spectra of the u_1 and u_2 fluctuations in the two flows.

The modulus of $C_{12}(\omega, \mathrm{y}, 0)$, which is equal to the square root of the coherence of frequency components of u_1 and u_2, varies less than the shear stress coefficient

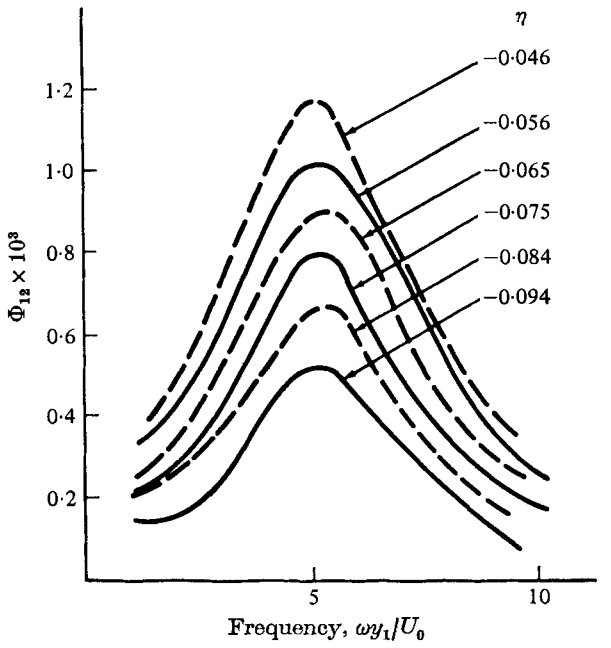

FIGURE 14. Shear stress spectrum at a number of positions on the high velocity edge of the mixing layer. $y_1 = 27$ cm, $U_0 = 12\,\mathrm{m\,s^{-1}}$.

$$\int_0^\infty \Phi_{12}(\omega)\, d\omega y_1/U_0 = \overline{u_1 u_2}/U_0^2.$$

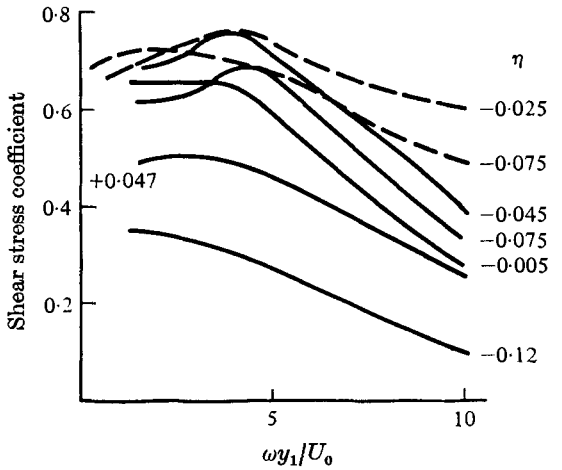

FIGURE 15. Shear stress coefficient, which is the real part of C_{12} $(\omega, y, 0)$, at a number of positions across the mixing layer. $y_1 = 27$ cm, $U_0 = 12\,\mathrm{m\,s^{-1}}$. ----, Bradshaw *et al.* (1964).

across the mixing layer (i.e. there is more order in the velocity fluctuations than the simple shear stress coefficient indicates). This is particularly true near the edges of the flow, where u_1 and u_2 components are quite coherent, but make a small contribution to the shear stress because the phase angle $\theta_{12}(\omega)$ in figure 16 shows they are nearly in quadrature.

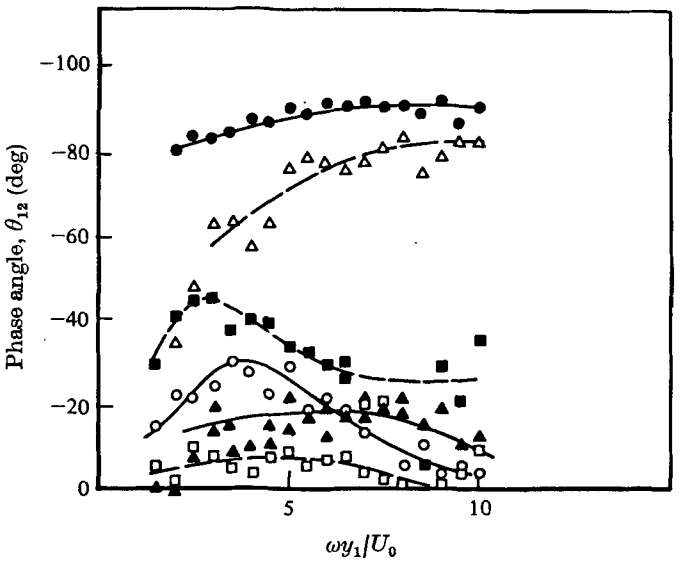

FIGURE 16. Phase angle of $C_{12}(\omega, \mathbf{y}, 0)$ at a number of positions across the mixing layer. Negative angles imply u_2 leads u_1. $y_1 = 27$ cm, $U_0 = 12\,\mathrm{m\,s^{-1}}$.

η	+0·047	0	−0·045	−0·075	−0·120	−0·22
	■	○	□	▲	△	●

In order to compute the wavenumber frequency spectrum, the filtered correlation $C_{12}(\omega, \mathbf{y}, r_1)$ was measured for separations in the downstream direction. These filtered correlations show clearly that they do not, in general, reach a maximum at $r_1 = 0$, but rather at some positive value of r_1, where the phase angles are close to zero. The modulus of $C_{12}(\omega, \mathbf{y}, r_1)$, on the other hand, does appear to have a maximum at $r_1 = 0$ (at least for positive r_1). For this reason, the advantage of fitting the filtered correlation with the form of (6) is evident, since the modulus of $C_{12}(\omega, \mathbf{y}, r_1)$ can be assumed symmetrical in r_1 without assuming the real part of the correlation to be symmetrical in r_1. The assumption of symmetry is still in error, to the extent that the characteristic scales increase with y_1.

The wavenumber transform calculated from the filtered correlation $C_{12}(\omega, \mathbf{y}, \mathbf{r})$ is in general complex, because the phase angle of the correlation is non-zero at $\mathbf{r} = 0$. It follows from our fitting function of (6) that, for a phase angle at $r_1 = 0$ of $\theta_{12}(\omega, 0)$,

$$\mathrm{Re}\,[M_{12}(k_1, \omega)] = |M_{12}(k_1, \omega)| \cos\theta_{12}(\omega, 0),$$

$$\mathrm{Im}\,[M_{12}(k_1, \omega)] = |M_{12}(k_1, \omega)| \sin\theta_{12}(\omega, 0).$$

The phase angles are available in figure 16, while the modulus of $M_{12}(k_1, \omega)$ is plotted in figures 17 and 18 for two positions on the high-velocity side of the mixing layer. The modulus of $M_{12}(k_1, \omega)$ is of course real, and it has the property

$$|M_{12}(k_1, \omega)| = |M_{12}(-k_1, -\omega)|,$$

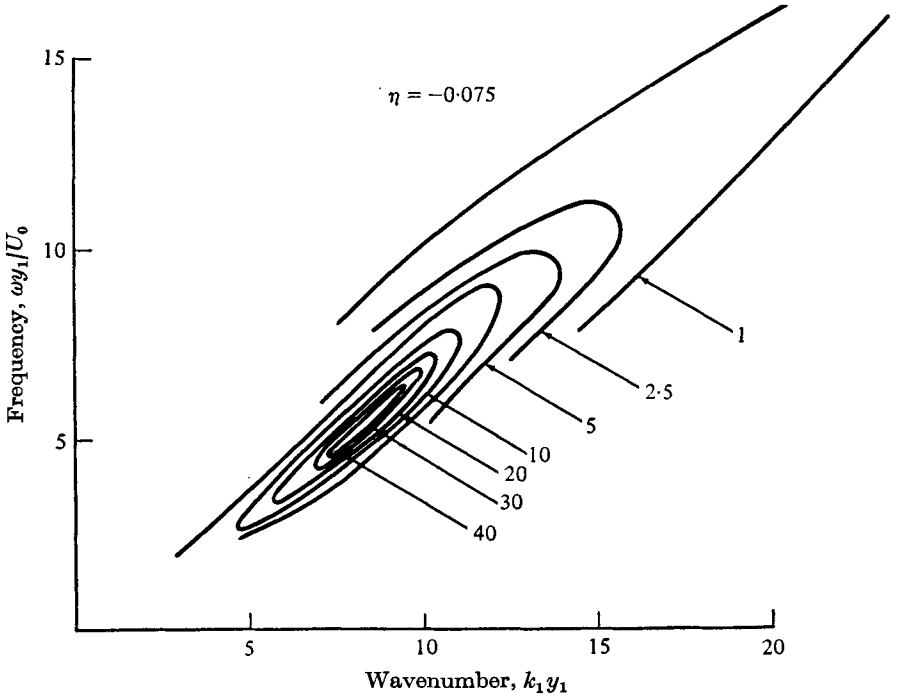

FIGURE 17. Contours of the modulus of the wavenumber frequency spectrum $M_{12}(k_1, \omega) \times 10^3$ at $\eta = -0{\cdot}075$, $y_1 = 27$ cm, $U_0 = 12\,\mathrm{m\,s^{-1}}$.

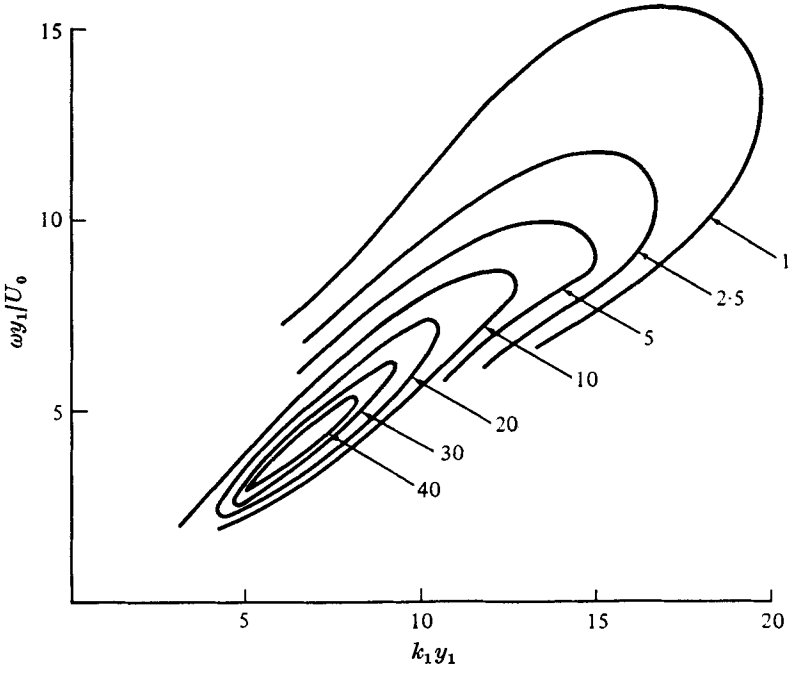

FIGURE 18. Contours of the modulus of the wavenumber frequency spectrum $M_{12}(k_1, \omega) \times 10^3$ at $\eta = -0{\cdot}046$, $y_1 = 27$ cm, $U_0 = 12\,\mathrm{m\,s^{-1}}$.

since $|C_{12}(\omega, \mathbf{y}, r_1)|$ is even. Thus, the spectra are presented only for positive frequencies, and they are normalized so that

$$\int_0^\infty \int_{-\infty}^\infty M_{12}(k_1, \omega)\, dk_1 y_1\, d\omega y_1 / U_0 = 1. \tag{14}$$

The modulus of $M_{12}(k_1, \omega)$ does not have the above property, but $\mathrm{Re}\,[M_{12}(k_1, \omega)]$ does integrate to unity.

The $|M_{12}(k_1, \omega)|$ spectrum at $\eta = -0{\cdot}075$ is quite similar to the $M_{22}(k_1, \omega)$ spectrum at the same position, which is shown in figure 12. The convection velocities deduced from the M_{12}, M_{11} and M_{22} spectra are all about 0·75 of the local mean velocity. The convection velocities near the peak in the spectrum at $\eta = -0{\cdot}046$ are slightly less than those at $\eta = -0{\cdot}075$, and the energy is more widely distributed at higher frequencies. These two spectra are used in §5 to compute the lateral gradient of $M_{12}(k_1, \omega)$.

5. The maintenance of shear stress

Phillips (1967, 1969) suggested that in turbulent shear flows the Reynolds stress results from the direct interaction of the lateral turbulent fluctuations with the mean velocity gradient. The shear stress gradient across the flow is brought about by lateral fluctuations close to the point where their convection speed equals the local mean velocity. The increment of shear stress between y_2 and $y_2 + \delta y_2$ must have the same convection velocity as the lateral fluctuations at the matched layer (i.e. the local mean velocity between y_2 and $y_2 + \delta y_2$).

In order to test this requirement of the Phillips model we have calculated the difference between the modulus of the two shear stress spectra at $\eta = -0{\cdot}075$ and $\eta = -0{\cdot}046$ in figures 17 and 18. The resultant spectrum is shown in figure 22; it has been normalized so that

$$\int_0^\infty \int_{-\infty}^\infty \frac{\partial}{\partial \eta} |M_{12}(k_1, \omega)|\, dk_1 y_1 \frac{d\omega y_1}{U_0} = 1. \tag{15}$$

The region in k_1, ω space that corresponds to convection velocities between the mean velocity at $\eta = -0{\cdot}075$ and $\eta = -0{\cdot}046$ is shown shaded in figure 19. The spectrum required is actually the gradient of the real part of $M_{12}(k_1, \omega)$, but the difference between this quantity and that in figure 19 is small, as can be seen by examining the phase angles shown in figure 16.

Most of the change in shear stress indicated in figure 19 has a convection velocity below that of the local mean. The convection velocity of $\partial/\partial y_2\, \overline{u_1 u_2}$ is closer to the convection velocity of the most energetic components of u_1 and u_2 than to the local mean speed. It appears from figure 19 that the matched layer contributes something less than a quarter of the total shear stress gradient in this region of the mixing layer. Most of the shear stress increment in figure 19 is travelling at speeds below the local mean where lateral fluctuations induce vorticity fluctuations which, Phillips argues, should be nearly in quadrature with the lateral fluctuations. The present result suggests that the correlation between the vorticity and lateral velocity away from the matched layer is large enough

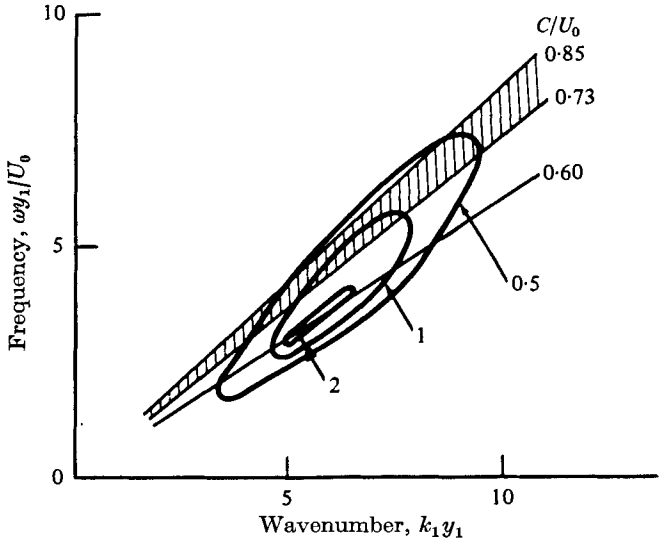

FIGURE 19. Contours of wavenumber frequency spectrum of the shear stress gradient. $\eta = -0{\cdot}075$, $y_1 = 27$ cm, $U_0 = 12\,\mathrm{m\,s^{-1}}$.

that, when it is applied to the most energetic components of the lateral velocity, it is these components that dominate the stress gradient.

This correlation coefficient is a complex function of the local turbulence field, since its introduction is a device to avoid solving the equations governing the interaction of the perturbation velocity with the turbulent stresses. Miles (1967) points out that this equation cannot be solved without *ad hoc* assumptions about the relationship between vorticity fluctuations and Reynolds stress.

With the present data we are able to evaluate the shear stress predicted by Phillips on the basis of this matched layer model. In the present notation, Phillips' (1969, (4.7)) expression for lateral shear gradient is

$$\frac{\partial}{\partial y_2}\overline{u_1 u_2} = \pi \frac{\partial^2 U}{\partial y_2^2}\overline{u_2^2}\int_{-\infty}^{\infty} \frac{k_1^2}{k_1^2+k_3^2}\frac{y_1}{U_0}\hat{M}_{22}(k_1, k_3, \omega_c)\,dk_1 y_1\,dk_3 y_3.$$

Here the frequency ω_c of the wavenumber component k_1 travelling at the local mean U is

$$\omega_c = Uk_1.$$

A structure constant may be defined as

$$\beta = 2\int_{-\infty}^{\infty} \frac{k_1^2}{k_1^2+k_3^2}\hat{M}_{22}(k_1, k_3, \omega_c)\,dk_1\,dk_3 \Big/ \left[\int_{-\infty}^{\infty} \hat{M}_{22}(k_1, k_3, \omega_c)\,dk_1\,dk_3\right], \quad (16)$$

and a time scale as

$$2\Theta_{22} = \frac{y_1\pi}{U_0}\int_{-\infty}^{\infty} \hat{M}_{22}(k_1, k_3, \omega_c)\,dk_1 y_1\,dk_3 y_1 = \frac{y_1\pi}{U_0}\int_{-\infty}^{\infty} \hat{M}_{22}(k_1, \omega_c)\,dk_1 y_1. \quad (17)$$

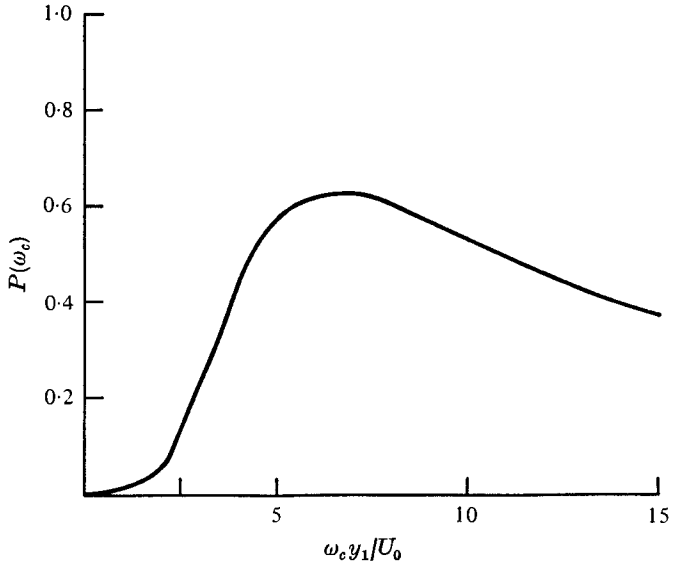

FIGURE 20. Integrand in lateral velocity structure constant.
$\eta = -0{\cdot}075$, $y_1 = 27\,\mathrm{cm}$, $U_0 = 12\,\mathrm{m\,s^{-1}}$.

Expression (17) contains a factor of 2π omitted by Phillips. This gives

$$\frac{\partial}{\partial y_2}\overline{u_1 u_2} = \overline{u_2^2}\beta\frac{\partial^2 U_1}{\partial y_2^2}\Theta_{22}, \tag{18}$$

on substitution into Phillips (1969, (4.7)).

If $\overline{u_2^2}\beta\Theta_{22}$ is a weak function of y_2, (18) can be integrated to give

$$\overline{u_1 u_2} = \overline{u_2^2}\beta\Theta_{22}\frac{\partial U}{\partial y_2}. \tag{19}$$

The term $\overline{u_2^2}\beta\Theta_{22}$ has the form of an eddy viscosity, which was found to be reasonably constant across the mixing layer by Wygnanski & Fiedler (1970).

The structure constant β has been evaluated from the appropriate measurements at $\eta = -0{\cdot}075$, using the assumption that the three-dimensional spectrum can be constructed from the measured two-dimensional spectrum, as in (9). Under this separation, the structure constant becomes

$$\beta = 2\frac{\int_{-\infty}^{\infty} M_{22}(k_1,\omega_c)\int_{-\infty}^{\infty}\frac{k_1^2}{k_1^2+k_3^2}M_{22}(k_3,\omega_c)\,dk_3\,dk_1}{\left[\int_{-\infty}^{\infty} M_{22}(k_1,\omega_c)\int_{-\infty}^{\infty} M_{22}(k_3,\omega_c)\,dk_3\,dk_1\right]}.$$

The inner integral, which we shall write as

$$P(\omega_c) = \frac{y_1}{\phi_{22}(\omega_c)}\int_{-\infty}^{\infty}\frac{k_1^2}{k_1^2+k_3^2}M_{22}(k_3,\omega_c)\,dk_3,$$

was evaluated from the results in figure 13 and is shown in figure 20. Using the $M_{22}(k_1,\omega)$ spectrum of figure 12, β was calculated to be 1·0.

If the $M_{22}(k_1,\omega_c)$ spectrum was concentrated at $k_3 = 0$ so that $k_1^2/(k_1^2+k_3^2)$ could

$\dfrac{\overline{u_1 u_2}}{U_0^2}$ measured	$\dfrac{\overline{u_2^2}}{U_0^2}$	β	$\dfrac{y_1}{U_0}\dfrac{\partial U}{\partial y_2}$	$\dfrac{U_0}{y_1}\Theta_{22}$	$\dfrac{\overline{u_1 u_2}}{U_0^2}$ equation (19)
0·0072	0·0156	1·0	4·0	0·07	0·0044

TABLE 1. Properties of mixing layer, $\eta = -0{\cdot}075$

be approximated by unity, $P(\omega_c)$ would also be unity, and β would equal 2. Since the wavenumber spectrum has a peak in the k_1 direction (equivalent to the observation that the space correlation in the downstream direction has a negative loop), and $P(\omega_c)$ is order one half at this value of k_1, the structure function is order unity.

The other parameter in (19) is the time constant θ_{22} defined by (17), which, as Phillips (1967) pointed out, is equal to the integral time scale in a frame of reference moving with velocity U. It is not in general equal to the time scale determined in a frame reference moving at such a speed as to optimize the time scale. This optimizing frame of reference was used by Davies, Fisher & Barratt (1963), Wygnanski & Fiedler (1970) and others to calculate the analogous longitudinal velocity time scale. Davies *et al.* (1963) found this optimum time scale to be 4·5 $(\partial U/\partial y_2)^{-1}$, where $\partial U/\partial y_2$ is the local mean velocity gradient. Wygnanski & Fiedler (1970) did not find the same dependence on mean velocity gradient, but that at $\eta = -0{\cdot}075$ the optimum longitudinal velocity time scale was $0{\cdot}37 y_1/U_0$. For the lateral velocity using the $M_{22}(k_1, \omega)$ spectrum in figure 12, the optimum time scale is $0{\cdot}33\ y_1/U_0$ at $\eta = -0{\cdot}075$, while the time scale defined in (17), Θ_{22}, is $0{\cdot}07 y_1/U_0$. This time scale, in a frame of reference moving at the local mean, is obtained by performing the integration along the line $\omega/k = 0{\cdot}85 U_0$ where inspection of figure 12 shows there is much reduced spectral energy.

The measured values of the quantities necessary to evaluate (19) are either described above or available in Wygnanski & Fiedler (1970) and they are listed in table 1. These values of turbulent intensity, etc., when substituted into (19), account for 60% of the measured shear stress, but overestimate the fraction of the increment that occurs at the matched layer. This underestimation of the stress by the direct-interaction model, in the light of the errors introduced by separation of variables, is not very significant by itself. It is interesting, however, to compare this result with the observation of Miles (1967), that the stress supported at the critical layer in the atmosphere over ocean waves appears to be inadequate to explain the growth of much of the ocean wave energy.

Another approach, that leads to some small insight into the problem of shear stress maintenance away from the matched layer, is to transform the inviscid momentum equation into Fourier space, and multiply it by the Fourier component of the lateral velocity fluctuations. For an idealized mixing layer with only one mean velocity $U_1 = U$, and one mean velocity gradient $\partial U/\partial y_2$, conservation of momentum leads to

$$\frac{\partial u_i}{\partial t} + u_2 \frac{\partial U}{\partial y_2} + U \frac{\partial u_i}{\partial y_1} + \sum_k \frac{\partial}{\partial y_k} (u_1 u_k)' = -\frac{\partial p}{\partial y_i}. \tag{20}$$

p is the fluctuating pressure, and $(u_i, u_j)'$ the fluctuating stress. A Fourier transform into wavenumber frequency components of (20) for $i = 1$, in the manner of the inverse of

$$u_i(\mathbf{y}, t) = \int_{-\infty}^{\infty}\int_{-\infty}^{\infty} \exp(+i\omega t - ik_1 y_1)\, Z_i(k_1, \omega, \mathbf{y})\, d\omega\, dk_1,$$

leads to $$i\omega Z_1 - ik_1 U Z_1 + Z_2 \frac{\partial U}{\partial y_2} - ik_1 Z_{11} + \frac{\partial}{\partial y_2} Z_{12} + \frac{\partial}{\partial y_3} Z_{13} + \frac{\partial \Pi}{\partial y_1} = 0.$$

$\Pi(k_1, \omega)$ is the transform of the pressure term, and Z_{1k} is the transform of the fluctuating stress $(u_1 u_k)'$. If we multiply this expression by Z_2^*, we obtain

$$ik_1\left(\frac{\omega}{k_1} - U\right) Z_1 Z_2^* + \underbrace{Z_2 Z_2^* \frac{\partial U}{\partial y_2}}_{\text{generation}} - \underbrace{ik_1 Z_{11} Z_2^*}_{\text{nonlinear term}}$$

$$+ \underbrace{\left[Z_2^* \frac{\partial}{\partial y_2} Z_{12} + Z_2^* \frac{\partial}{\partial y_3} Z_{13} + Z_2^* \frac{\partial \Pi}{\partial y_1}\right]}_{\text{pressure and remaining nonlinear terms}} = 0. \qquad (21)$$

On multiplying (21) by $dk_1 d\omega$ and ensemble-averaging it, we finally obtain

$$ik_1\left(\frac{\omega}{k_1} - U\right) M_{12}(k_1, \omega) + M_{22}(k_1, \omega)\frac{\partial U}{\partial y_2} - ik_1 M_{11,2}$$

$$+ \left\{\begin{matrix}\text{pressure and remaining} \\ \text{nonlinear terms}\end{matrix}\right\} = 0. \qquad (22)$$

The shear stress spectrum $M_{12}(k_1, \omega)$ is predominantly real. (The phase angles in figure 16 are small, except near the edges of the mixing layer.) Thus, the first term in (22), $ik_1(\omega/k_1 - U)\, M_{12}$, is largely imaginary. The $M_{22}(k_1, \omega)$ spectrum in the generation term is real and so, away from the matched layer (i.e. ω/k_1 not equal to U), the generation term cannot contribute directly to the real part of the shear stress spectrum. The imaginary part of the shear stress spectrum, while not zero, does not contribute to the shear stress. The real part of the shear stress spectrum for components travelling at velocities other than U results from the transfer of energy from the generation term to the nonlinear and pressure terms. These latter terms are, in general, complex and so can act as a coupling mechanism to drive Z_1 components in phase with the Z_2 components extracting energy from the mean flow.

In figure 21 we have plotted the real and imaginary terms in (22) for one frequency as measured at $\eta = -0{\cdot}075$. The pressure and remaining nonlinear (triple product) terms in (22) were obtained by the difference between the first three terms. At the matched layer for this frequency, i.e. near a wavenumber of $k_1 y_1 = 5{\cdot}9$, the production term has dropped to a small fraction of its maximum value. It should be noted that (22) neglects any terms that result from the spreading of the mixing layer.

If the gradient of the real part of $M_{12}(k_1, \omega)$ was to be zero away from the matched layer, then the gradients of the imaginary part of the nonlinear and pressure terms would have to be zero and the gradients of the generation term

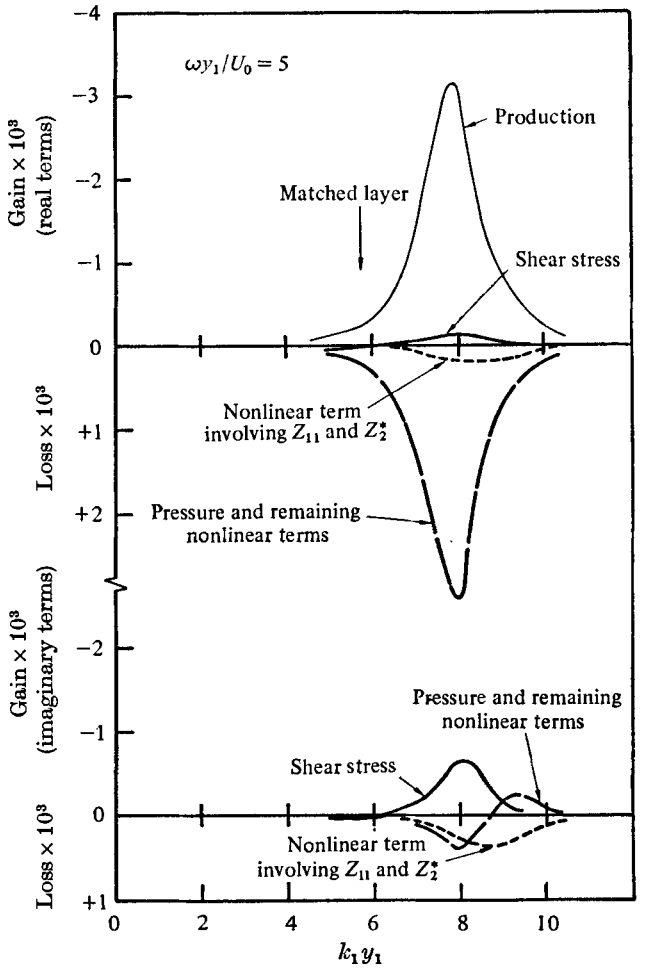

FIGURE 21. Terms in the transformed momentum equation (22) for a fixed frequency. $\eta = -0{\cdot}075$, $y_1 = 27$ cm, $U_0 = 12\,\mathrm{m\,s^{-1}}$.

would have to be balanced by the real part of the pressure and nonlinear terms. The one nonlinear term that was measured, $ikM_{11,2}$, has a substantial imaginary part and it is not unreasonable to expect significant lateral gradients in this and the other nonlinear terms. More extensive measurements would be required to prove this point but it does seem likely that the gradients in the nonlinear terms support the observed gradient of shear stress away from the matched layer. Terms such as the triple products of velocities are neglected in Phillips' model of direct interaction of lateral fluctuation with the mean velocity.

6. Conclusions

By assuming homogeneity of the lateral and longitudinal velocity fluctuations in a mixing layer, the two-dimensional cross spectrum was measured, and its lateral gradient on the high velocity side of the mixing layer was used to show that

the major portion of the increment in shear stress occurs away from the matched layer.

Phillips' direct-interaction model, when evaluated from the three-dimensional spectrum under the same assumption of homogeneity, together with the assumption that it can be adequately described by the separation of variables used in this paper, gave a value equal to about 60 % of the total shear stress at $\eta = -0{\cdot}075$.

The evaluation assumed that the coefficient between lateral fluctuations and vorticity at the matched layer was π, the value in laminar flow. If this coefficient was somewhat reduced for the present turbulent flow, the predicted shear stress increment at the matched layer could be made to agree adequately with that observed in figure 19.

Fluctuations travelling at other than the local mean appear to be able to support significant shear stress gradients, and it is the nonlinear terms in the momentum equation that play an important role in correlating the lateral and longitudinal fluctuations in a manner that contributes to the shear stress.

Thus it appears that, in the mixing layer, direct-interaction models between mean flow and lateral fluctuations are not very successful. Possibly in flows with lower turbulence intensities (at $\eta = -0{\cdot}075$ the r.m.s. turbulence level was 0·16 of the local mean), the nonlinear terms are less important. However, one is not encouraged by the lack of success in predicting ocean-wave generation by means of critical layer models.

The computation of spectra and the digitization of the data relied heavily on the techniques developed by Dr Y. H. Pao, and the results presented were dependent on specific computer programs written by Mr S. D. Hansen.

Appendix. Definition of some spectral transforms

$$R_{ij}(\mathbf{r},t) = \frac{\overline{u_i(\mathbf{y},\tau)\,u_j(\mathbf{y}+\mathbf{r},\tau+t)}}{\overline{u_i(\mathbf{y},\tau)\,u_j(\mathbf{y},\tau)}}.$$

Here we assume homogeneity in $\mathbf{y}$ and τ,

$$\phi_{ij}(\omega) = \frac{U_0}{\pi y_1}\int_{-\infty}^{\infty} R_{ij}(0,t)\exp(-i\omega t\,dt),$$

$$R_{ij}(0,t) = \int_0^{\infty} \phi_{ij}(\omega)\exp(i\omega t)\frac{d\omega y_1}{U_0},$$

$$M_{ij}(k_m,\omega) = \frac{U_0}{2\pi^2 y_1^2}\int_{-\infty}^{\infty} R_{ij}(r_m,t)\exp(ik_m r_m - i\omega t)\,dr_m dt,$$

$$\int_0^{\infty}\int_{-\infty}^{\infty} M_{ij}(k_m,\omega)\,dk_m y_1 \frac{d\omega y_1}{U_0} = 1,$$

$$\hat{M}_{ij}(k_1,k_3,\omega) = \frac{U_0}{4\pi^3 y_1^3}\int_{-\infty}^{\infty} R_{ij}(r_1,r_3,t)\exp(ik_1 r_1 + ik_3 r_3 - i\omega t)\,dr_1 dr_3 dt.$$

Note: no summation on repeated indices.

REFERENCES

BATT, R. G., KUBOTA, T. & LAUFER, J. 1970 Experimental investigation of the effect of shear flow turbulence on a chemical reaction. *A.I.A.A. Paper*, no. 70–721.

BRADSHAW, P. & FERRISS, D. H. 1965 The spectral energy balance in a turbulent mixing layer. *Nat. Phys. Lab. Aero. Rep.* no. 1144.

BRADSHAW, P., FERRISS, D. H. & JOHNSON, R. F. 1964 Turbulence in the noise-producing region of a circular jet. *J. Fluid Mech.* **19**, 591.

DAVIES, P. O. A. L., FISHER, M. J. & BARRATT, M. J. 1963 The characteristics of turbulence in the mixing region of a round jet. *J. Fluid Mech.* **15**, 337.

JONES, I. S. F. 1968 Scales pertinent to noise generation from a jet. *AFOSR–UTIAS Symp. on Aerodynamic Noise*, p. 69. Toronto University Press.

JONES, I. S. F. 1969 Fluctuating turbulent stresses in the noise-producing region of a jet. *J. Fluid Mech.* **36**, 529.

LIEPMANN, H. W. & LAUFER, J. 1947 Investigations of free turbulent mixing. *N.A.C.A. Tech. Note*, no. 1257.

LUMLEY, J. L. & PANOFSKY, H. A. 1964 *The Structure of Atmospheric Turbulence.* Wiley.

MILES, J. W. 1957 On the generation of surface waves by shear flow. *J. Fluid Mech.* **3**, 185.

MILES, J. W. 1967 On the generation of surface waves by shear flows. Part 5. *J. Fluid Mech.* **30**, 163.

PHILLIPS, O. M. 1967 The maintenance of Reynolds stress in turbulent shear flow. *J. Fluid Mech.* **27**, 131.

PHILLIPS, O. M. 1969 Shear-flow turbulence. *Ann. Rev. Fluid Mech.* **1**, 245.

WILLS, J. A. B. 1964 On convection velocities in turbulent shear flows. *J. Fluid Mech.* **20**, 417.

WILLS, J. A. B. 1971 Measurements for wavenumber/phase velocity spectrum of wall pressure beneath a turbulent boundary layer. *J. Fluid Mech.* **45**, 65.

WYGNANSKI, I. & FIEDLER, H. E. 1970 The two-dimensional mixing region. *J. Fluid Mech.* **41**, 327.